


Cite this: *RSC Adv.*, 2023, 13, 15410

# Facile formation of barium titanium oxyhydride on a titanium hydride surface as an ammonia synthesis catalyst†

Yoshihiro Goto,<sup>a</sup> Masashi Kikugawa,<sup>a</sup> Keisuke Kobayashi,<sup>b</sup> Yuichi Manaka,<sup>b</sup> Tetsuya Nanba,<sup>b</sup> Hideyuki Matsumoto,<sup>bc</sup> Mitsuru Matsumoto,<sup>a</sup> Masakazu Aoki<sup>a</sup> and Haruo Imagawa<sup>a</sup>

Oxyhydrides are promising compounds as supports for ammonia synthesis catalysts because they suppress hydrogen poisoning on the catalyst surface and enhance the ammonia synthesis activity. Herein, we developed a facile method for preparing BaTiO<sub>2.5</sub>H<sub>0.5</sub>, a perovskite oxyhydride, on a TiH<sub>2</sub> surface via the conventional wet impregnation method using TiH<sub>2</sub> and Ba hydroxide. Scanning electron microscopy and high-angle annular dark-field scanning transmission electron microscopy observations revealed that BaTiO<sub>2.5</sub>H<sub>0.5</sub> crystallized as nanoparticles of ca. 100–200 nm on the TiH<sub>2</sub> surface. The Ru-loaded catalyst Ru/BaTiO<sub>2.5</sub>H<sub>0.5</sub>-TiH<sub>2</sub> exhibited 2.46 times higher ammonia synthesis activity (3.05 mmol-NH<sub>3</sub> g<sup>-1</sup> h<sup>-1</sup> at 400 °C) than the benchmark Ru catalyst Ru-Cs/MgO (1.24 mmol-NH<sub>3</sub> g<sup>-1</sup> h<sup>-1</sup> at 400 °C) because of the suppression of hydrogen poisoning. The analysis of reaction orders showed that the effect of suppressing hydrogen poisoning on Ru/BaTiO<sub>2.5</sub>H<sub>0.5</sub>-TiH<sub>2</sub> was equivalent to that of the reported Ru/BaTiO<sub>2.5</sub>H<sub>0.5</sub> catalyst, thus supporting the formation of BaTiO<sub>2.5</sub>H<sub>0.5</sub> perovskite oxyhydride. This study demonstrated that the selection of appropriate raw materials facilitates the formation of BaTiO<sub>2.5</sub>H<sub>0.5</sub> oxyhydride nanoparticles on the TiH<sub>2</sub> surface using the conventional synthesis method.

Received 8th March 2023  
Accepted 17th May 2023

DOI: 10.1039/d3ra01539d

rsc.li/rsc-advances

## Introduction

Ammonia (NH<sub>3</sub>), an essential raw material in the production of agricultural fertilizers and synthetic chemicals, has recently attracted attention owing to its applicability as a hydrogen carrier or fuel.<sup>1,2</sup> Ammonia is predominantly produced *via* the Haber–Bosch (HB) process, which accounts for 1–2% of the global energy demand and 2.5% of global CO<sub>2</sub> emissions.<sup>3</sup> Most of the CO<sub>2</sub> emissions are responsible for hydrogen production processes using steam reforming (CH<sub>4</sub> + H<sub>2</sub>O → CO + 3H<sub>2</sub>) and water gas shift reactions (CO + H<sub>2</sub>O → CO<sub>2</sub> + H<sub>2</sub>). Replacing these processes with water electrolysis (2H<sub>2</sub>O → 2H<sub>2</sub> + O<sub>2</sub>) using renewable energy can significantly reduce this CO<sub>2</sub> emission.<sup>4</sup> However, renewable electricity sources of an intermittent nature are not compatible with ammonia synthesis *via* the conventional HB process<sup>5</sup> because the process is operated on large-scale and steady-state operations. On this basis, ammonia

synthesis catalysts need severe reaction conditions (at 450–600 °C and 15–40 MPa).<sup>5</sup> Therefore, ammonia synthesis catalysts that work under mild conditions should be developed for ammonia synthesis using renewable electricity sources.

The rate-determining step in the synthesis of ammonia (3H<sub>2</sub> + N<sub>2</sub> → 2NH<sub>3</sub>) is the dissociation of the N<sub>2</sub> triple bond (945 KJ mol<sup>-1</sup>), which is the strongest bond among those in diatomic molecules.<sup>6,7</sup> Supported ruthenium (Ru) catalysts are the most promising candidates for ammonia synthesis under mild conditions because optimum N<sub>2</sub> adsorption energy facilitates N<sub>2</sub> dissociation on the Ru surface.<sup>8</sup> Strongly basic supports (such as CeO<sub>2</sub>, La<sub>0.5</sub>Pr<sub>0.5</sub>O<sub>1.75</sub>, Ba/Ce<sub>0.5</sub>La<sub>0.5</sub>O<sub>1.75</sub>, CeO<sub>2</sub>-PrO<sub>x</sub>, and Ce<sub>0.5</sub>La<sub>0.5-x</sub>Ti<sub>x</sub>O<sub>1.75+0.5x</sub>)<sup>9–14</sup> further promote N<sub>2</sub> dissociation because the basic compounds enhance the electron transfer from the Ru metal to the antibonding orbital of N<sub>2</sub>.<sup>15</sup> However, hydrogen atoms generated by H<sub>2</sub> dissociation are often adsorbed on the active sites of the Ru surface, thereby preventing N<sub>2</sub> dissociation on the Ru surface.<sup>16</sup> In recent years, oxyhydrides such as BaTiO<sub>3-x</sub>H<sub>x</sub>, BaCeO<sub>3-x</sub>H<sub>y</sub>N<sub>z</sub>, LaH<sub>3-2x</sub>O<sub>x</sub>, GdHO, and SmHO have been reported as supports that suppress hydrogen poisoning and enhance the ammonia synthesis activity of Ru catalysts.<sup>17–20</sup> Suppression of hydrogen poisoning is presumed to originate from the diffusivity of hydride (H<sup>-</sup>), which allows hydrogen spillover from the Ru metal to the surface of the oxyhydride supports.<sup>21</sup>

<sup>a</sup>Toyota Central R&D Labs., Inc., 41-1 Yokomichi, Nagakute 480-1192, Aichi, Japan.  
E-mail: yoshihiro-goto@mosk.tytlabs.co.jp

<sup>b</sup>Renewable Energy Research Center, National Institute of Advanced Industrial Science and Technology, 2-2-9 Machiikedai, Koriyama 963-0298, Fukushima, Japan

<sup>c</sup>Department of Chemical Science and Engineering, School of Materials and Chemical Technology, Tokyo Institute of Technology, 2-12-1 Ookayama, Meguro-ku, Tokyo, 152-8552, Japan

† Electronic supplementary information (ESI) available. See DOI: <https://doi.org/10.1039/d3ra01539d>



Transition-metal (TM) oxyhydride synthesis is generally complicated because the differences in chemical properties (such as reactivity, volatility, and ionic radius) among anions prevent different anions in an identical compound from becoming stable.<sup>22</sup> For this reason, solid-state topochemical reactions and/or high-pressure reactions have been used to synthesize TM oxyhydrides.<sup>22</sup> BaTiO<sub>3-x</sub>H<sub>x</sub>, which is a promising TM perovskite oxyhydride support for ammonia synthesis catalysts, cannot be prepared by simply reducing BaTiO<sub>3</sub> with hydrogen. However, this oxyhydride is accessible *via* a solid-state topochemical reaction involving BaTiO<sub>3</sub> and CaH<sub>2</sub> because the reaction can provide a metastable phase by exchanging the oxide (O<sup>2-</sup>) in BaTiO<sub>3</sub> with hydride (H<sup>-</sup>) in CaH<sub>2</sub> while maintaining the basic framework structure of BaTiO<sub>3</sub>.<sup>23</sup> However, materials preparation using the topochemical reaction is not suitable for practical use because the reaction involves a multi-step process: (1) mixing BaTiO<sub>3</sub> and the moisture-sensitive CaH<sub>2</sub> in an inert atmosphere, (2) calcining the mixture for a week under vacuum, and (3) washing in an inert atmosphere to extract product BaTiO<sub>3-x</sub>H<sub>x</sub> by removing the residual CaH<sub>2</sub> and by-product CaO. The practical utility of BaTiO<sub>3-x</sub>H<sub>x</sub> may be limited by low producibility owing to the multi-step process. Thus, developing more facile, efficient ways to prepare BaTiO<sub>3-x</sub>H<sub>x</sub> is necessary to accelerate the application of BaTiO<sub>3-x</sub>H<sub>x</sub>. Moreover, the development can lead to the discovery of novel oxyhydrides.

Recently, Uchimura *et al.*<sup>24</sup> have reported the direct synthesis of BaTiO<sub>3-x</sub>H<sub>x</sub> by a mechanochemical method using BaH<sub>2</sub>, BaO, and TiO<sub>2</sub> and confirmed its performance as a hydrogen-permeable electrode. However, handling in an inert atmosphere is still required because BaH<sub>2</sub> and BaO are sensitive to moisture. Herein, we demonstrated the synthesis of BaTiO<sub>3-x</sub>H<sub>x</sub> ( $x = 0.5$ ), a perovskite oxyhydride, on a TiH<sub>2</sub> surface *via* conventional wet impregnation method using TiH<sub>2</sub> and Ba(OH)<sub>2</sub>·8H<sub>2</sub>O, which are stable in moisture and air. The obtained BaTiO<sub>2.5</sub>H<sub>0.5</sub> was crystallized as fine particles of 100–200 nm size that covered the TiH<sub>2</sub> particle surface. The Ru-loaded catalyst, Ru/BaTiO<sub>2.5</sub>H<sub>0.5</sub>-TiH<sub>2</sub>, showed 2.46 times higher ammonia synthesis activity than Ru-Cs/MgO as benchmark Ru catalyst. Moreover, Ru/BaTiO<sub>2.5</sub>H<sub>0.5</sub>-TiH<sub>2</sub> suppressed hydrogen poisoning, thereby proving the formation of BaTiO<sub>2.5</sub>H<sub>0.5</sub> perovskite oxyhydride.

## Methods

BaTiO<sub>2.5</sub>H<sub>0.5</sub>-TiH<sub>2</sub> was synthesized *via* the wet impregnation method using TiH<sub>2</sub> powder and Ba hydroxide solution. TiH<sub>2</sub> (98%, –325 mesh, Sigma-Aldrich) was impregnated with a solution containing the desired amount of Ba(OH)<sub>2</sub>·8H<sub>2</sub>O (98.0%, FUJIFILM Wako Chemicals) dissolved in 3 : 2 (v/v) H<sub>2</sub>O/ethanol at 230 °C in the air, after which it was heated at 350 °C for 3 h in a 10% H<sub>2</sub>/N<sub>2</sub> atmosphere. The Ba addition amounts were varied from 0–15 wt% on a Ba(OH)<sub>2</sub> basis. The obtained compounds are hereafter referred to as Ba( $\alpha$ )-TiH<sub>2</sub> ( $\alpha$ : wt% of Ba(OH)<sub>2</sub>). Reference compounds Ba( $\alpha$ )-TiO<sub>2</sub> (where  $\alpha$  = wt% of Ba(OH)<sub>2</sub>) were prepared using the same protocols as for Ba( $\alpha$ )-TiH<sub>2</sub>, except TiO<sub>2</sub> (99.9%, Rutile, Sigma-Aldrich) was used

instead of TiH<sub>2</sub>. Ba(10)-TiH<sub>2</sub> synthesized using Ba(CH<sub>3</sub>COO)<sub>2</sub> (99.0%, FUJIFILM Wako Chemicals) or Ba(NO<sub>3</sub>)<sub>2</sub> (99.0%, FUJIFILM Wako Chemicals) instead of Ba(OH)<sub>2</sub>·8H<sub>2</sub>O were also prepared to investigate the effect of Ba sources. Cs/MgO as a benchmark compound was prepared by impregnation using MgO (99%, Sigma-Aldrich) and Cs<sub>2</sub>CO<sub>3</sub> (99.9%, Sigma-Aldrich)/ethanol solution, followed by thermal treatment at 350 °C for 3 h under 10% H<sub>2</sub>/N<sub>2</sub>. Ru-loaded catalysts, such as Ru/Ba( $\alpha$ )-TiH<sub>2</sub>, Ru/Ba( $\alpha$ )-TiO<sub>2</sub>, and Ru-Cs/MgO, were prepared by impregnation using Ru<sub>3</sub>(CO)<sub>12</sub> (99%, Sigma-Aldrich)/tetrahydrofuran solution. The suspension was stirred for 5 h, and the solvent was subsequently evaporated at 27 °C. The obtained compound was dried at 80 °C for 16 h in the air. The Cs and Ru loading amounts were 1 wt% on a metal basis.

X-ray diffraction (XRD) patterns were collected at room temperature using SmartLab (Rigaku) with Cu K $\alpha$  radiation ( $\lambda = 1.54056$  Å). The obtained XRD patterns were analyzed using the JANA2006 software.<sup>25</sup> The neutron diffraction (ND) pattern was collected at room temperature using the NOVA time-of-flight (TOF) neutron diffractometer at the J-PARC facility in Japan. The obtained ND pattern was analyzed using Z-Rietveld software.<sup>26</sup> Fourier-transform infrared (FT-IR) spectra were recorded using an iS50 spectrometer (Thermo Fisher) equipped with a diffuse reflectance optics accessory. Samples were pretreated at 200 °C for 30 min in flowing He and then examined at 50 °C. Scanning electron microscopy (SEM) images were obtained using a JSM-7400F (JEOL) and a SU3500 (Hitachi) operated at 1.5 kV. High-angle annular dark-field scanning transmission electron microscopy (HAADF-STEM) and energy-dispersive X-ray spectroscopy (EDS) mapping images were obtained using a Tecnai Osiris (FEI) operated at 200 kV. X-ray photoelectron spectroscopy (XPS) was conducted on a Quantera SXM instrument (ULVAC PHI) using Al K $\alpha$  radiation (1486.6 eV). CO amounts adsorbed by the catalyst were estimated using a BEL-METAL-3 (MicrotracBEL). CO pulse injections (1.99% CO/He) to the samples were conducted at 50 °C after the pretreatment at 400 °C for 2 h in 100% H<sub>2</sub>.

The ammonia synthesis activities under ambient pressure were estimated using a fixed-bed reactor connected to mass flow controllers. A sample (0.2 g) was suspended on a bed of quartz wool in a quartz tube and preheated at 400 °C for 2 h in 75% H<sub>2</sub>/N<sub>2</sub> (H<sub>2</sub>/N<sub>2</sub> = 3) at a flow rate of 80 mL min<sup>-1</sup>. The activity measures were conducted at 300–400 °C in 75% H<sub>2</sub>/N<sub>2</sub> (H<sub>2</sub>/N<sub>2</sub> = 3) at a flow rate of 80 mL min<sup>-1</sup>. The ammonia concentrations in the outlet of the quartz tube were monitored by FT-IR spectroscopy and converted into ammonia synthesis rates. Reaction orders of ammonia synthesis with respect to H<sub>2</sub>, N<sub>2</sub>, and NH<sub>3</sub> were estimated using the method of Aika *et al.*<sup>27</sup>

## Results and discussion

The XRD patterns of Ba( $\alpha$ )-TiH<sub>2</sub> ( $\alpha = 0, 1, 3, 5, 10$ , and 15) predominantly showed the cubic phase of the fluorite structure ( $Fm\bar{3}m$ ) with the lattice parameter of  $a = 4.4489$ – $4.4519$  Å (Fig. 1). The lattice parameter matches that of the reported TiH<sub>2</sub> ( $a = 4.4512(1)$  Å),<sup>28</sup> showing that the cubic phase is TiH<sub>2</sub>. The XRD patterns of samples with  $\alpha = 0$  and 1 only showed the



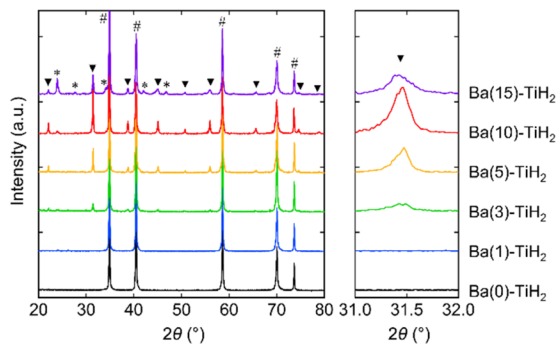


Fig. 1 XRD patterns of Ba( $\alpha$ )-TiH<sub>2</sub> ( $\alpha$  = 0, 1, 3, 5, 10, and 15). Hashtags (#), triangles (▼), and asterisks (\*) indicate peaks arising from TiH<sub>2</sub>, BaTiO<sub>2.5</sub>H<sub>0.5</sub>, and BaCO<sub>3</sub>, respectively.

single phase of TiH<sub>2</sub>, whereas the XRD patterns of  $\alpha \geq 3$  samples contained an additional cubic phase of perovskite structure ( $Pm\bar{3}m$ ; Fig. S1 in the ESI†). The lattice volume was estimated to be  $V = 64.926\text{--}65.073 \text{ \AA}^3$  (Table 1), which approaches that reported for cubic BaTiO<sub>2.38</sub>H<sub>0.62</sub> perovskite oxyhydride ( $Pm\bar{3}m$ ,  $V = 65.140 \text{ \AA}^3$ )<sup>23</sup> rather than tetragonal BaTiO<sub>3</sub> perovskite oxide ( $P4mm$ ,  $V = 64.281 \text{ \AA}^3$ ),<sup>29</sup> which indicates that the additional cubic phase is BaTiO<sub>3-x</sub>H<sub>x</sub> perovskite oxyhydride. The H content  $x$  in BaTiO<sub>3-x</sub>H<sub>x</sub> ( $\alpha$  = 3, 5, 10, and 15) were determined to be  $x = 0.47\text{--}0.57$  based on Vegard's law (Table 1; hereafter, the obtained perovskite oxyhydride is referred to as BaTiO<sub>2.5</sub>H<sub>0.5</sub>). The formation of oxygen-deficient BaTiO<sub>3- $\delta$</sub>  is unlikely because the lattice volume of BaTiO<sub>2.5</sub>H<sub>0.5</sub> ( $V = 64.926\text{--}65.073 \text{ \AA}^3$ ) is larger than that reported for cubic BaTiO<sub>3- $\delta$</sub>  perovskite oxide ( $\delta = 0.25$ ,  $Pm\bar{3}m$ ,  $V = 64.337 \text{ \AA}^3$ ) where the lattice volume does not change through the formation of oxygen defects.<sup>30</sup> The formation of the BaTiO<sub>3- $\delta$</sub> (OH) <sub>$\delta$</sub>  oxyhydroxide through OH<sup>-</sup> incorporation is also denied because no peaks associated with OH bonds (observed at  $3400 \text{ cm}^{-1}$  in BaTiO<sub>3</sub> system)<sup>31</sup> were observed by FT-IR spectroscopy (Fig. S2†). Moreover, the XRD patterns of the  $\alpha = 10$  and 15 samples showed that BaCO<sub>3</sub> can potentially form through the reaction of unreacted Ba(OH)<sub>2</sub> with atmospheric CO<sub>2</sub> absorbed during impregnation. Thus, the addition of Ba into TiH<sub>2</sub> forms BaTiO<sub>2.5</sub>H<sub>0.5</sub> perovskite oxyhydride and BaCO<sub>3</sub>.

Table 1 Physical characteristics of Ba( $\alpha$ )-TiH<sub>2</sub> ( $\alpha$  = 0, 1, 3, 5, 10, and 15)

Sample	Lattice volume of BaTiO <sub>3-x</sub> H <sub>x</sub> <sup>a</sup> ( $\text{\AA}^3$ )	H content $x$ <sup>b</sup>
Ba(0)-TiH <sub>2</sub>	—	—
Ba(1)-TiH <sub>2</sub>	—	—
Ba(3)-TiH <sub>2</sub>	65.002(2)	0.52
Ba(5)-TiH <sub>2</sub>	64.926(2)	0.47
Ba(10)-TiH <sub>2</sub>	65.009(2)	0.56
Ba(15)-TiH <sub>2</sub>	65.073(3)	0.57

<sup>a</sup> Calculated from the lattice parameters based on the cubic perovskite structure ( $Pm\bar{3}m$ ,  $Z = 1$ ). <sup>b</sup> Determined from Vegard's law using the lattice volumes of BaTiO<sub>3</sub> ( $V = 64.281 \text{ \AA}^3$ )<sup>29</sup> and BaTiO<sub>2.38</sub>H<sub>0.62</sub> ( $V = 65.140 \text{ \AA}^3$ ).<sup>23</sup>

The ND pattern of Ba(10)-TiH<sub>2</sub> was collected to investigate the presence of the hydride in BaTiO<sub>2.5</sub>H<sub>0.5</sub> (Fig. S3 and Table S1†). Rietveld refinement was performed by assuming that the secondary phase is a BaTiO<sub>3-x</sub>H<sub>x</sub> cubic perovskite with a  $Pm\bar{3}m$  structural model, where Ba, Ti, and O/H atoms are placed at the Wyckoff position of  $1a$  (0, 0, 0),  $1b$  (0.5, 0.5, 0.5), and  $3c$  (0, 0.5, 0.5), respectively. Cubic TiH<sub>2</sub> ( $Fm\bar{3}m$ ) was added as a primary phase. Refinement converged to O and H occupancies of  $g(\text{O}) = 0.886(2)$  and  $g(\text{H}) = 0.114(2)$ , which yields the BaTiO<sub>2.658(6)</sub>H<sub>0.342(6)</sub> composition and supports the notion that perovskite phase contains hydride. We note here that the difference in the neutron scattering lengths of oxygen and hydrogen (O: 5.803 fm, H: -3.741 fm)<sup>32</sup> gives the composition BaTiO<sub>2.438(6)</sub> when the refinement is performed by assuming that the secondary phase is oxygen-deficient BaTiO<sub>3- $\delta$</sub> . However, because the formation of oxygen-deficient BaTiO<sub>3- $\delta$</sub>  is ruled out by considering the lattice volumes estimated by the XRD analysis, the ND results support the formation of an oxyhydride.

The degrees of BaTiO<sub>2.5</sub>H<sub>0.5</sub> and BaCO<sub>3</sub> formation were determined by Rietveld refinement of the XRD patterns of Ba( $\alpha$ )-TiH<sub>2</sub>. We note here that components (less than about 1%) that are not detected in the XRD analysis are not considered. As shown in Fig. 2, the mass fraction of BaTiO<sub>2.5</sub>H<sub>0.5</sub> is 0% at  $0 \leq \alpha \leq 1$  and higher at  $3 \leq \alpha \leq 10$  (1.6% to 8.7%). However, a lower fraction was observed at  $\alpha = 15$  (4.5%). The addition of Ba to TiH<sub>2</sub> facilitates the formation of BaTiO<sub>2.5</sub>H<sub>0.5</sub>, while excess Ba inhibits its formation. Thus, the optimum amount of Ba(OH)<sub>2</sub> needed to form BaTiO<sub>2.5</sub>H<sub>0.5</sub> corresponds to  $\alpha = 10$ . The mass fraction of the formed BaCO<sub>3</sub> was 0% at  $0 \leq \alpha \leq 5$  but higher at  $10 \leq \alpha \leq 15$  (0.7 to 4.3%), which implies that unreacted Ba(OH)<sub>2</sub> remains at  $\alpha \geq 10$ . The samples also exhibited colors that depend on the amounts of BaTiO<sub>2.5</sub>H<sub>0.5</sub> and BaCO<sub>3</sub> amounts (Fig. S4†). Ba(0)-TiH<sub>2</sub> and Ba(5)-TiH<sub>2</sub> are gray, which is typical of TiH<sub>2</sub>, while Ba(10)-TiH<sub>2</sub> is dark blue, which is typical of BaTiO<sub>2.5</sub>H<sub>0.5</sub>,<sup>23</sup> which also supports the notion that the BaTiO<sub>2.5</sub>H<sub>0.5</sub> perovskite oxyhydride had formed. Ba(15)-TiH<sub>2</sub> is brown, which is possibly due to mixed colors associated with TiH<sub>2</sub>, BaTiO<sub>2.5</sub>H<sub>0.5</sub>, and BaCO<sub>3</sub>.

The SEM image of Ba(0)-TiH<sub>2</sub> revealed that the particle size of TiH<sub>2</sub> ranged from several to tens of  $\mu\text{m}$  (Fig. S5 and S6†). Particle size was not affected by the amount of added Ba, which

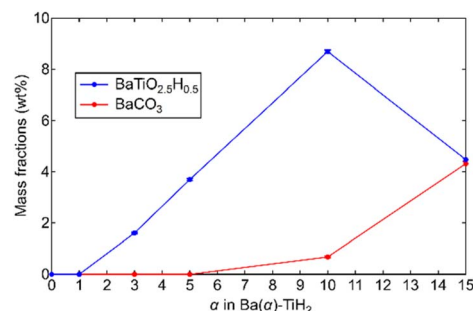


Fig. 2 Mass fractions of BaTiO<sub>2.5</sub>H<sub>0.5</sub> and BaCO<sub>3</sub> in Ba( $\alpha$ )-TiH<sub>2</sub> determined by Rietveld refinements of the XRD patterns of Ba( $\alpha$ )-TiH<sub>2</sub>. Cubic TiH<sub>2</sub> ( $Fm\bar{3}m$ ), cubic BaTiO<sub>2.5</sub>H<sub>0.5</sub> ( $Pm\bar{3}m$ ), and orthorhombic BaCO<sub>3</sub> ( $Pnma$ ) phases were applied during the analysis.



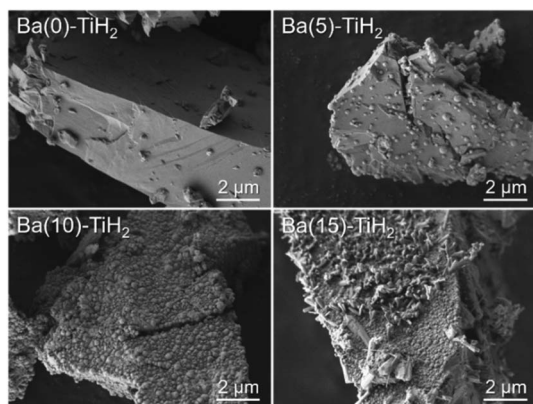


Fig. 3 SEM images of Ba( $\alpha$ )-TiH<sub>2</sub> ( $\alpha$  = 0, 5, 10, and 15) at 100 00× magnification.

agreed with the identical specific surface area of Ba( $\alpha$ )-TiH<sub>2</sub> ( $0 \leq \alpha \leq 15$ ;  $1.65\text{--}1.91\text{ m}^2\text{ g}^{-1}$ ). The particle surface of Ba(0)-TiH<sub>2</sub> and Ba(1)-TiH<sub>2</sub> were relatively smooth; by comparison, nanoparticles of *ca.* 100–200 nm were dispersed on the TiH<sub>2</sub> surface of Ba(3)-TiH<sub>2</sub> and Ba(5)-TiH<sub>2</sub> (Fig. 3). The nanoparticles were expected to be BaTiO<sub>2.5</sub>H<sub>0.5</sub> because BaTiO<sub>2.5</sub>H<sub>0.5</sub> in addition to TiH<sub>2</sub> was observed in the XRD patterns of Ba(3)-TiH<sub>2</sub> and Ba(5)-TiH<sub>2</sub> (Fig. 1). The EDX mappings in the HAADF-STEM image of Ru/Ba(5)-TiH<sub>2</sub> show that Ba and O elements were localized at the nanoparticles (Fig. 4), thus supporting the identification of the nanoparticles as BaTiO<sub>2.5</sub>H<sub>0.5</sub>. The Ba/Ti atomic ratio estimated from the XPS analysis was higher than that of the feed ratio in the preparation, also supporting that the nanoparticles are BaTiO<sub>2.5</sub>H<sub>0.5</sub>. The SEM image of Ba(10)-TiH<sub>2</sub> showed that the BaTiO<sub>2.5</sub>H<sub>0.5</sub> nanoparticles fully covered the TiH<sub>2</sub> particle. Moreover, the SEM image of Ba(15)-TiH<sub>2</sub> showed needle-shaped particles on the BaTiO<sub>2.5</sub>H<sub>0.5</sub> nanoparticles. The crystals were identified as BaCO<sub>3</sub> according to the XRD pattern because BaCO<sub>3</sub> generally formed needle-shape crystals.<sup>33</sup> Therefore, BaTiO<sub>2.5</sub>H<sub>0.5</sub> was formed as 100–200 nm nanoparticles at  $\alpha \geq 3$ , and BaCO<sub>3</sub> was formed as needle shape particles at  $\alpha \geq 10$  (Fig. 5).

The XRD patterns of Ba( $\alpha$ )-TiO<sub>2</sub> ( $\alpha$  = 0, 5, 10, 15) synthesized as comparison are shown in Fig. S8.† All samples showed

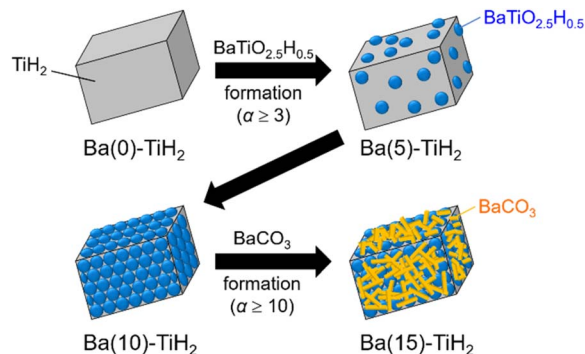


Fig. 5 Images of the morphological change of Ba( $\alpha$ )-TiH<sub>2</sub>.

predominantly rutile TiO<sub>2</sub>. Ba(0)-TiO<sub>2</sub> was the single phase of TiO<sub>2</sub>, whereas Ba( $\alpha$ )-TiO<sub>2</sub> ( $\alpha$  = 5, 10, and 15) contained additional Ba<sub>2</sub>TiO<sub>4</sub> and BaCO<sub>3</sub>. The cubic phase of BaTiO<sub>2.5</sub>H<sub>0.5</sub> formed in Ba( $\alpha$ )-TiH<sub>2</sub> was not observed with the addition of any amount of Ba(OH)<sub>2</sub>. Therefore, TiH<sub>2</sub> is essential for BaTiO<sub>2.5</sub>H<sub>0.5</sub> formation.

How is TiH<sub>2</sub> involved in the formation of BaTiO<sub>2.5</sub>H<sub>0.5</sub>? TiH<sub>2</sub> consumed to form BaTiO<sub>2.5</sub>H<sub>0.5</sub> is calculated to be 2.1% for Ba(10)-TiH<sub>2</sub> which contains the highest amount of BaTiO<sub>2.5</sub>H<sub>0.5</sub> (8.7%; Fig. 2), suggesting that only the surface part of the TiH<sub>2</sub> particles contributes to the formation. This is supported by the SEM and TEM observations (Fig. 3 and 4). Because metal hydrides are generally unstable in an oxidizing atmosphere, the surface of TiH<sub>2</sub> particles is known to be covered by an oxide film of TiO<sub>2</sub>.<sup>34</sup> TiH<sub>2</sub> (Ti<sup>2+</sup>) partially oxidized to TiO<sub>2</sub> (Ti<sup>4+</sup>) possibly contributes to the formation of BaTiO<sub>2.5</sub>H<sub>0.5</sub> (Ti<sup>3.5+</sup>) *via* the reaction  $\text{Ba(OH)}_2 + 0.5x\text{TiH}_2 + (1 - 0.5x)\text{TiO}_2 \rightarrow \text{BaTiO}_{3-x}\text{H}_x + \text{H}_2\text{O}$ . Moreover, the effect of Ba reagents on BaTiO<sub>2.5</sub>H<sub>0.5</sub> formation was investigated. The XRD patterns of Ba(10)-TiH<sub>2</sub> synthesized using Ba(CH<sub>3</sub>COO)<sub>2</sub> or Ba(NO<sub>3</sub>)<sub>2</sub> instead of Ba(OH)<sub>2</sub>·8H<sub>2</sub>O are shown in Fig. S9.† The XRD pattern of Ba(10)-TiH<sub>2</sub> synthesized *via* Ba(CH<sub>3</sub>COO)<sub>2</sub> showed only TiH<sub>2</sub> and Ba(CH<sub>3</sub>COO)<sub>2</sub> and no formation of BaTiO<sub>2.5</sub>H<sub>0.5</sub>. While Ba(10)-TiH<sub>2</sub> synthesized *via* Ba(NO<sub>3</sub>)<sub>2</sub> contained BaTiO<sub>2.5</sub>H<sub>0.5</sub>, its mass fraction (1.5%) was only 0.17-times that of the Ba(10)-TiH<sub>2</sub> synthesized *via* Ba(OH)<sub>2</sub>·8H<sub>2</sub>O (8.7%). These observations suggest that the hydroxide ion (OH<sup>−</sup>) promotes the formation of BaTiO<sub>2.5</sub>H<sub>0.5</sub>.

The ammonia synthesis activities of Ru/Ba( $\alpha$ )-TiH<sub>2</sub> ( $0 \leq \alpha \leq 15$ ) catalysts were examined at 300–400 °C under ambient pressure (Fig. 6a). Ammonia synthesis rates of all catalysts increased at elevated temperature. Ru/Ba(0)-TiH<sub>2</sub> exhibited ammonia synthesis activity at  $\geq 375$  °C. The ammonia synthesis rate of Ru/Ba(0)-TiH<sub>2</sub> ( $0.05\text{ mmol g}^{-1}\text{ h}^{-1}$  at 400 °C) was 0.04 times that of Ru/Cs–MgO ( $1.24\text{ mmol g}^{-1}\text{ h}^{-1}$  at 400 °C), which was often called as benchmark Ru catalysts.<sup>35,36</sup> The activity of Ru/Ba(1)-TiH<sub>2</sub> ( $0.20\text{ mmol g}^{-1}\text{ h}^{-1}$  at 400 °C) was higher than that of Ru/Ba(0)-TiH<sub>2</sub> but remained lower than that of Ru/Cs–MgO. However, by contrast, the activities of Ru/Ba(3)-TiH<sub>2</sub>, Ru/Ba(5)-TiH<sub>2</sub>, and Ru/Ba(10)-TiH<sub>2</sub> ( $1.73$ ,  $2.08$ , and  $3.05\text{ mmol g}^{-1}\text{ h}^{-1}$  at 400 °C, respectively) were higher than that of Ru–Cs/MgO by a factor of 1.40, 1.68, and 2.46, respectively. Activity increased

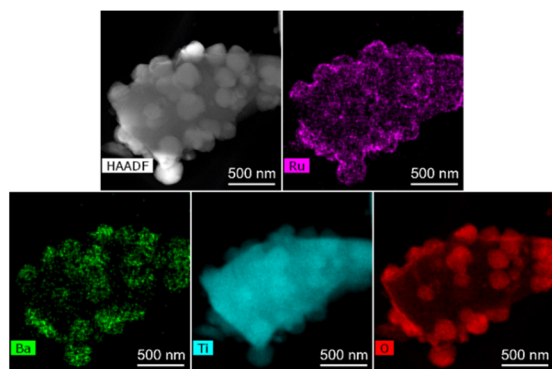


Fig. 4 STEM-HAADF and EDX mapping images of Ru/Ba(5)-TiH<sub>2</sub>.

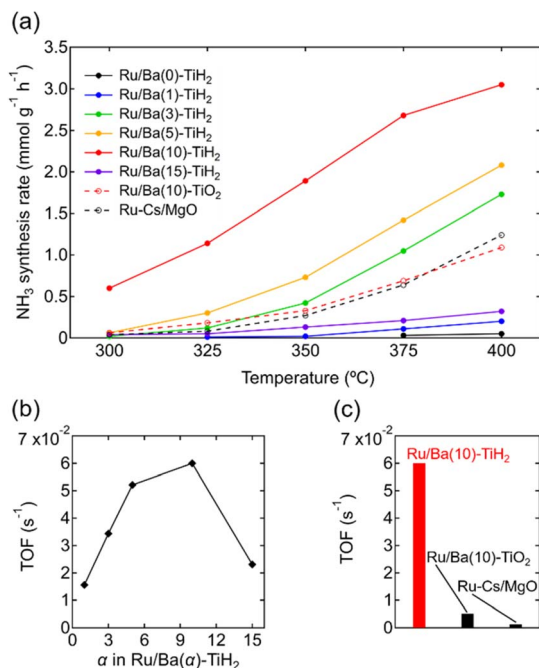


Fig. 6 (a) Temperature dependence of the NH<sub>3</sub> synthesis rates for Ru/Ba(α)-TiH<sub>2</sub> (α = 0, 1, 3, 5, 10, and 15), Ru/Ba(10)-TiO<sub>2</sub>, and Ru-Cs/MgO (reaction conditions: catalyst, 0.2 g; reaction gas, H<sub>2</sub>/N<sub>2</sub> = 3 at a flow rate of 80 mL min<sup>-1</sup>; pressure = ambient pressure). (b) TOF of Ru/Ba(α)-TiH<sub>2</sub> (α = 0, 1, 3, 5, 10, and 15) at 350 °C as functions of Ba(OH)<sub>2</sub> added amount α. (c) TOF of Ru/Ba(10)-TiH<sub>2</sub>, Ru/Ba(10)-TiO<sub>2</sub>, and Ru-Cs/MgO at 350 °C.

with the increase in Ba addition amount in  $0 \leq \alpha \leq 10$ , whereas the activity decreased at  $\alpha = 15$  ( $0.32 \text{ mmol g}^{-1} \text{ h}^{-1}$  at 400 °C). Therefore, the most active catalyst among Ru/Ba(α)-TiH<sub>2</sub> ( $0 \leq \alpha \leq 15$ ) was Ru/Ba(10)-TiH<sub>2</sub>. The activity of Ru/Ba(10)-TiH<sub>2</sub> was higher than that of Ru/Ba(10)-TiO<sub>2</sub> ( $1.09 \text{ mmol g}^{-1} \text{ h}^{-1}$  at 400 °C), thereby suggesting that BaTiO<sub>2.5</sub>H<sub>0.5</sub> formation was responsible for the high activity of Ru/Ba(10)-TiH<sub>2</sub>.

The TOF for the ammonia synthesis reaction at 350 °C was estimated to obtain a deeper insight into the correlation between ammonia synthesis activity and catalyst composition. As shown in Fig. 6b, the TOF of Ru/Ba(α)-TiH<sub>2</sub> increased with increasing amount of Ba addition at  $1 \leq \alpha \leq 10$  ( $1.56 \times 10^{-2} \text{ s}^{-1}$  to  $6.00 \times 10^{-2} \text{ s}^{-1}$ ) but decreased at  $\alpha = 15$  ( $2.31 \times 10^{-2} \text{ s}^{-1}$ ). This trend was consistent with the trend of the mass fraction of BaTiO<sub>2.5</sub>H<sub>0.5</sub> (Fig. 2); these observations support that BaTiO<sub>2.5</sub>H<sub>0.5</sub> formation contributes to the increase in ammonia synthesis activity. This was supported by the fact that the TOF of Ru/Ba(10)-TiH<sub>2</sub> ( $6.00 \times 10^{-2} \text{ s}^{-1}$ ) was 12 and 46 times larger than those of Ru/Ba(10)-TiO<sub>2</sub> ( $0.51 \times 10^{-2} \text{ s}^{-1}$ ) and Ru-Cs/MgO ( $0.13 \times 10^{-2} \text{ s}^{-1}$ ), respectively (Fig. 6c). Interestingly, the TOF of Ru/Ba(15)-TiH<sub>2</sub> ( $2.31 \times 10^{-2} \text{ s}^{-1}$ ) was lower than that of Ru/Ba(5)-TiH<sub>2</sub> ( $5.21 \times 10^{-2} \text{ s}^{-1}$ ) despite the higher mass fraction of BaTiO<sub>2.5</sub>H<sub>0.5</sub> for Ru/Ba(15)-TiH<sub>2</sub> (4.48%) than that for Ru/Ba(5)-TiH<sub>2</sub> (3.70%). The formation of BaCO<sub>3</sub>, which partially covered the BaTiO<sub>2.5</sub>H<sub>0.5</sub> particles (Fig. 3), was expected to inhibit the ammonia synthesis reaction of Ru/Ba(15)-TiH<sub>2</sub> because BaCO<sub>3</sub> was stable in the reaction temperature.<sup>37</sup>

Table 2 Reaction orders<sup>a</sup> for ammonia synthesis reaction over Ru/Ba(10)-TiH<sub>2</sub> and Ru-Cs/MgO

Catalyst	Order		
	H <sub>2</sub>	N <sub>2</sub>	NH <sub>3</sub>
Ru/Ba(10)-TiH <sub>2</sub>	0.15	0.79	-0.36
Ru-Cs/MgO	-0.59	0.89	0.11

<sup>a</sup> Estimated from results of kinetic analysis shown in Fig. S8.

Finally, reaction orders with respect to H<sub>2</sub>, N<sub>2</sub> and NH<sub>3</sub> were investigated using the method of Aika *et al.*<sup>27</sup> (Fig. S10 and Table S3<sup>†</sup>). The H<sub>2</sub> order of Ru/Ba(10)-TiH<sub>2</sub> (0.15) was higher than that of Ru-Cs/MgO (-0.59), reflecting that compared to Ru-Cs/MgO, Ru/Ba(10)-TiH<sub>2</sub> had less hydrogen poisoning, which prevented N<sub>2</sub> dissociation on Ru (Table 2).<sup>16</sup> The low hydrogen poisoning effect allowed Ru/Ba(10)-TiH<sub>2</sub> to exhibit higher ammonia synthesis activity than Ru-Cs/MgO. The N<sub>2</sub> orders of Ru/Ba(10)-TiH<sub>2</sub> (0.79) and Ru-Cs/MgO (0.89) were virtually coincident, reflecting that the rate-determining step for both catalysts was the unimolecular cleavage reaction of N<sub>2</sub> for both catalysts. Moreover, the orders of Ru/Ba(10)-TiH<sub>2</sub> (H<sub>2</sub> order: 0.15, N<sub>2</sub> order: 0.79) agreed well with the reported orders of Ru/BaTiO<sub>2.5</sub>H<sub>0.5</sub> (H<sub>2</sub> order: 0.2, N<sub>2</sub> order: 0.7).<sup>17</sup> Because Ru/BaTiO<sub>3</sub>, the reference catalyst for Ru/BaTiO<sub>2.5</sub>H<sub>0.5</sub>, exhibits stronger hydrogen poisoning due to the absence of hydride in the support perovskite (H<sub>2</sub> order: -0.89, N<sub>2</sub> order: 1.2),<sup>17</sup> the agreement of the H<sub>2</sub> and N<sub>2</sub> orders between Ru/Ba(10)-TiH<sub>2</sub> and Ru/BaTiO<sub>2.5</sub>H<sub>0.5</sub> supports the formation of BaTiO<sub>2.5</sub>H<sub>0.5</sub> in Ru/Ba(10)-TiH<sub>2</sub>. The NH<sub>3</sub> order of Ru/Ba(10)-TiH<sub>2</sub> (-0.36) was higher than that reported for Ru/BaTiO<sub>2.5</sub>H<sub>0.5</sub> (-0.64), indicating that the ammonia decomposition reaction on Ru/Ba(10)-TiH<sub>2</sub> was relatively inhibited. The inhibition may be attributed to the reaction pressure of this study (ambient pressure) being lower than that of reported Ru/BaTiO<sub>2.5</sub>H<sub>0.5</sub> (5 MPa) because the ammonia decomposition reaction generally proceeded at a higher pressure.<sup>38</sup>

## Conclusions

The selection of appropriate raw materials allowed for BaTiO<sub>2.5</sub>H<sub>0.5</sub> perovskite oxyhydride nanoparticles to be formed on the TiH<sub>2</sub> surface through the conventional wet impregnation method. BaTiO<sub>2.5</sub>H<sub>0.5</sub> crystallized as *ca.* 100–200 nm sized nanoparticles on the surface of TiH<sub>2</sub>. Hydroxide in Ba(OH)<sub>2</sub> involved BaTiO<sub>2.5</sub>H<sub>0.5</sub> formation. Ru-loaded catalysts inhibited hydrogen poisoning and showed higher ammonia synthesis activity compared to that of the Ru-Cs/MgO benchmark catalyst. We believe that further investigation of oxyhydride prepared *via* the wet impregnation method accelerates the use of oxyhydride as ammonia synthesis catalysts.

## Author contributions

Yoshihiro Goto: conceptualization, investigation, writing – original draft, Masashi Kikugawa: investigation, Keisuke



Kobayashi: data curation, Yuichi Manaka: validation, Tetsuya Nanba: conceptualization, project administration, Hideyuki Matsumoto: formal analysis Mitsuru Matsumoto: validation, Masakazu Aoki: supervision, project administration, Haruo Imagawa: supervision, writing-review & editing.

## Conflicts of interest

There are no conflicts to declare.

## Acknowledgements

The authors acknowledge Mr Akira Takatsuki (National Institute of Advanced Industrial Science and Technology, Ibaraki, Japan) for his contribution in collecting the SEM and STEM-HAADF images.

## Notes and references

- J. W. Erisman, M. A. Sutton, J. Galloway, Z. Klimont and W. Winiwarter, *Nat. Geosci.*, 2008, **1**, 636.
- A. Klerke, C. H. Christensen, J. K. Nørskov and T. Vegge, *J. Mater. Chem.*, 2008, **18**, 2304.
- P. H. Pfromm, *J. Renewable Sustainable Energy*, 2017, **9**, 034702.
- C. Smith, A. K. Hill and L. Torrente-Murciano, *Energy Environ. Sci.*, 2020, **13**, 331.
- M. Ravi and J. W. Makepeace, *Chem. Sci.*, 2022, **13**, 890.
- S. Gambarotta and J. Scott, *Angew. Chem., Int. Ed.*, 2004, **43**, 5298.
- K. Honkala, A. Hellman, I. N. Remediakis, A. Logadottir, A. Carlsson, S. Dahl, C. H. Christensen and J. K. Nørskov, *Science*, 2005, **307**, 555.
- C. J. H. Jacobsen, S. Dahl, B. S. Clausen, S. Bahn, A. Logadottir and J. K. Nørskov, *J. Am. Chem. Soc.*, 2001, **123**, 8404.
- Y. Niwa and K. Aika, *Chem. Lett.*, 1996, **3**, 3.
- Y. Ogura, K. Tsujimaru, K. Sato, S. Miyahara, T. Toriyama, T. Yamamoto, S. Matsumura and K. Nagaoka, *ACS Sustainable Chem. Eng.*, 2018, **6**, 17258.
- Y. Ogura, K. Sato, S. Miyahara, Y. Kawano, T. Toriyama, T. Yamamoto, S. Matsumura, S. Hosokawa and K. Nagaoka, *Chem. Sci.*, 2018, **9**, 2230.
- K. Sato, S. Miyahara, Y. Ogura, K. Tsujimaru, Y. Wada, T. Toriyama, T. Yamamoto, S. Matsumura and K. Nagaoka, *ACS Sustainable Chem. Eng.*, 2020, **8**, 2726.
- M. Kikugawa, Y. Goto, K. Kobayashi, T. Nanba, H. Matsumoto and H. Imagawa, *J. Catal.*, 2022, **413**, 934.
- Y. Goto, M. Kikugawa, K. Kobayashi, T. Nanba, H. Matsumoto and H. Imagawa, *Chem. Commun.*, 2022, **58**, 3210.
- K. Aika, A. Ohya, A. Ozaki, Y. Inoue and I. Yasumori, *J. Catal.*, 1985, **92**, 305.
- Y. Kadowaki and K. Aika, *J. Catal.*, 1996, **161**, 178.
- Y. Tang, Y. Kobayashi, N. Masuda, Y. Uchida, H. Okamoto, T. Kageyama, S. Hosokawa, F. Loyer, K. Mitsuhashi, K. Yamanaka, Y. Tamenori, C. Tassel, T. Yamamoto, T. Tanaka and H. Kageyama, *Adv. Energy Mater.*, 2018, **8**, 1801772.
- M. Kitano, J. Kujirai, K. Ogasawara, S. Matsuishi, T. Tada, H. Abe, Y. Niwa and H. Hosono, *J. Am. Chem. Soc.*, 2019, **141**, 20344.
- K. Ooya, J. Li, K. Fukui, S. Iimura, T. Nakao, K. Ogasawara, M. Sasase, H. Abe, Y. Niwa, M. Kitano and H. Hosono, *Adv. Energy Mater.*, 2021, **11**, 2003723.
- H. Yamashita, T. Broux, Y. Kobayashi, F. Takeiri, H. Ubukata, T. Zhu, M. A. Hayward, K. Fujii, M. Yashima, K. Shitara, A. Kuwabara, T. Murakami and H. Kageyama, *J. Am. Chem. Soc.*, 2018, **140**, 11170.
- K. Wang, Z. Wu and D. Jiang, *Phys. Chem. Chem. Phys.*, 2022, **24**, 1496.
- H. Kageyama, K. Hayashi, K. Maeda, J. P. Attfield, Z. Hiroi, J. M. Rondinelli and K. R. Poeppelmeier, *Nat. Commun.*, 2018, **9**, 772.
- Y. Kobayashi, O. J. Hernandez, T. Sakaguchi, T. Yajima, T. Roisnel, Y. Tsujimoto, M. Morita, Y. Noda, Y. Mogami, A. Kitada, M. Ohkura, S. Hosokawa, Z. Li, K. Hayashi, Y. Kusano, J. E. Kim, N. Tsuji, A. Fujiwara, Y. Matsushita, K. Yoshimura, K. Takegoshi, M. Inoue, M. Takano and H. Kageyama, *Nat. Mater.*, 2012, **11**, 507.
- T. Uchimura, F. Takeiri, K. Okamoto, T. Saito, T. Kamiyama and G. Kobayashi, *J. Mater. Chem. A*, 2021, **9**, 20371.
- V. Petříček, M. Dušek and L. Palatinus, *Z. Kristallogr. Cryst. Mater.*, 2004, **229**, 345.
- R. Oishi, M. Yonemura, Y. Nishimaki, S. Torii, A. Hoshikawa, T. Ishigaki, T. Morishima, K. Mori and T. Kamiyama, *Nucl. Instrum. Methods Phys. Res. A: Accel. Spectrom. Detect. Assoc. Equip.*, 2009, **600**, 94.
- K. Aika, M. Kumasaka, T. Oma, O. Kato, H. Matsuda, N. Watanabe, K. Yamazaki, A. Ozaki and T. Onishi, *Appl. Catal.*, 1986, **28**, 57.
- P. E. Kalita, S. V. Sinogeikin, K. E. Lipinska-Kalita, T. Hartmann, X. Ke, C. Chen and A. L. Cornelius, *J. Appl. Phys.*, 2010, **108**, 043511.
- R. H. Buttner and E. N. Maslen, *Acta Crystallogr.*, 1992, **B48**, 764.
- I.-K. Jeong, S. Lee, S. Jeong, C. J. Won, N. Hur and A. Llobet, *Phys. Rev. B*, 2011, **84**, 064125.
- P. R. Arya, P. Jha and A. K. Ganguli, *J. Mater. Chem.*, 2003, **13**, 415.
- V. F. Sears, *Neutron News*, 1992, **2**, 26.
- B. Sreedhar, Ch. Satya Vani, D. Keerthi Devi, V. Sreeram and M. V. Basaveswara Rao, *Am. J. Mater. Sci.*, 2012, **2**, 105.
- K. B. Park, J. H. Choi, T. W. Na, J. W. Kang, K. S. Park and H. K. Park, *Metals*, 2019, **9**, 1154.
- K. Aika, H. Hori and A. Ozaki, *J. Catal.*, 1972, **27**, 424.
- F. Rosowski, A. Hornung, O. Hinrichsen, D. Herein, M. Muhler and G. Ertl, *Appl. Catal.*, 1997, **151**, 443.
- X. Zhang, Q. Ye, B. Xu and D. He, *Catal. Lett.*, 2007, **117**, 140.
- F. Hayashi, Y. Toda, Y. Kanie, M. Kitano, Y. Inoue, T. Yokoyama, M. Hara and H. Hosono, *Chem. Sci.*, 2013, **4**, 3124.

